Lichter, S. G., M. C. Escudie, A. D. Stacey, K. Ganesan, K. Fox, A. Ahnood, N. V. Apollo, D. C. Kua, A. Z. Lee, C. McGowan, A. L. Saunders, O. Burns, D. A. Nayagam, R. A. Williams, D. J. Garrett, H. Meffin, and S. Prawer. 2015. Hermetic diamond capsules for biomedical implants enabled by gold active braze alloys. *Biomaterials*. **53**: 464-74.

doi: 10.1016/j.biomaterials.2015.02.103

Hermetic diamond capsules for biomedical implants enabled by gold active braze alloys

Samantha G. Lichter,[1] Mathilde C. Escudié,[1] Alastair D. Stacey,[1] Kumaravelu Ganesan,[1] Kate Fox,[2] Arman Ahnood,[1] Nicholas V. Apollo,[1] Dunstan C. Kua,[1,3] Aaron Z. Lee,[1,3] Ceara McGowan,[4] Alexia L. Saunders,[4] Owen Burns,[4] David A.X. Nayagam,[4,6] Richard A. Williams,[5,7] David J. Garrett,[1,4,*] Hamish Meffin,[5] Steven Prawer[1]

[1] *School of Physics, The University of Melbourne, Victoria 3010, Australia*

[2] *School of Aerospace, Mechanical and Manufacturing Engineering, RMIT University, Victoria 3001, Australia*

[3]*Department of Materials Engineering, Faculty of Engineering, Monash University, Victoria 3800, Australia*

[4] *The Bionics Institute, 384-388 Albert Street, East Melbourne, Victoria 3002, Australia*

[5] *National Vision Research Institute, Department of Optometry and Vision Sciences, University of Melbourne, Victoria 3010, Australia*

[6] *Department of Pathology, The University of Melbourne, Victoria 3010, Australia*

[7] *Department of Anatomical Pathology, St Vincent's Hospital, Fitzroy, Victoria 3065, Australia*

**Corresponding Author: David J. Garrett, dgarrett@unimelb.edu.au, Ph: +61403353730*

Abstract

As the field of biomedical implants matures the functionality of implants is rapidly increasing. In the field of neural prostheses this is particularly apparent as researchers strive to build devices that interact with highly complex neural systems such as vision, hearing, touch and movement. A retinal implant, for example, is a highly complex device and the surgery, training and rehabilitation requirements involved in deploying such devices are extensive. Ideally, such devices will be implanted only once and will continue to function effectively for the lifetime of the patient. The first and most pivotal factor that determines device longevity is the encapsulation that separates the sensitive electronics of the device from the biological environment. This paper describes the realisation of a free standing device encapsulation made from diamond, the most impervious, long lasting and biochemically inert material known. A process of laser micro-machining and brazing is

described detailing the fabrication of hermetic electrical feedthroughs and laser weldable seams using a 96.4% gold active braze alloy, another material renowned for biochemical longevity. Accelerated ageing of the braze alloy, feedthroughs and hermetic capsules yielded no evidence of corrosion and no loss of hermeticity. Samples of the gold braze implanted for 15 weeks, *in vivo*, caused minimal histopathological reaction and results were comparable to those obtained from medical grade silicone controls. The work described represents a first account of a freestanding, fully functional hermetic diamond encapsulation for biomedical implants, enabled by gold active alloy brazing and laser micro-machining.

Introduction

The medical bionics field is currently in a very exciting stage of growth. The success of the cochlear implant, restoring hearing to hundreds of thousands of patients by electrically stimulating sensory neurons in the auditory pathway, has been a major inspiration in the field. Newer generations of implanted devices, such as visual prostheses, aim to interact with neural tissue in complex ways, with hundreds or even thousands of stimulating electrodes, [1-3] based on the premise that higher electrode density and number will confer more information to the nervous system. Experience with the cochlear implant has also shown that the individual control of electrodes is essential, as tuning of each electrode is key to providing patients an optimised experience with their device. Accordingly, Bionic Vision Australia is currently developing a high acuity visual prosthesis with the aim of up to 1024 individually controlled stimulating electrodes.

Unfortunately, the momentum towards high electrode counts in implantable prostheses have created a major materials design problem. The electronic components in bionic implants, which are at risk of leaching unsafe materials into the tissue, and of suffering corrosion damage from exposure to moisture and ions, must be isolated within a hermetic encapsulation. It is commonly acknowledged that hermetic encapsulation is one of the major challenges for high resolution visual prostheses. [4-7] The most common approach to hermetic encapsulation, a vessel of titanium or ceramic with a ceramic feedthrough plate containing an array of brazed wires, is reaching its natural limit in electrode density. The risk of brittle cracking failure for each penetrating feedthrough increases as the feedthroughs get smaller and closer together. [8] Some are addressing this limitation by improving the ceramic technology, using screen-printing and co-fired ceramics to make high-density feedthrough

arrays. [9-11] These arrays can be hermetic with densities up to 2500 channels per square centimetre, [10] but they do not address the other obstacle of having high electrode counts: the flexible cable joining the feedthrough to the electrodes. A cable carrying hundreds or thousands of wires becomes an untenable prospect, due to issues such as stiffness and the risk of breakage in the fine wires. As the current materials of encapsulation are unlikely to provide an outlook for next generation hermetic miniaturised bionic implants, a new paradigm is required. Any new materials for encapsulation must be able to demonstrate their hermeticity to protect electronics, their durability to remain functional during chronic implantation, and their biocompatibility for safe and comfortable implantation.

Diamond has been hailed as the biomaterial of the 21st century. [12] While its high hardness, wear resistance and thermal conductivity are well known, recognition is now spreading for its chemical inertness which confers both biocompatibility [13-16] and biostability. [17] Diamond is also highly impermeable, as it is intrinsically non-porous, and diamond films grown by chemical vapour deposition (CVD) are pinhole-free after several hours of growth. [17] Xiao et al. showed that diamond films were provided a hermetic seal over silicon wafers which were not degraded after three months of implantation in the retinae of rabbits. Other advantages that diamond can offer for an implantable encapsulation are low density, so that capsules are light when fixed to fast-moving tissue such as the wall of the eye, and high strength, so that capsule walls can be thin for the sake of miniaturisation.

During the development of the Bionic Vision Australia's (BVA's) high acuity epiretinal prosthesis we have reported modification of and stimulation of retinal ganglion cell nerves with an activated form of nitrogen included ultananocrystalline diamond (N-UNCD) [18, 19]. We have also previously reported the use of N-UNCD to generated high density, hermetic feedthrough arrays suitable for direct integration with surface mount electronics and leading directly to a high density array of N-UNCD stimulating electrodes [20]. This paper describes a method to hermetically join a diamond capsule to our previously described diamond electrode array [20] using a gold based active braze alloy. Furthermore we show that the gold braze can also be used to generated low impedance feedthroughs in the box, suitable for data and power transfer to internal electronics. The components of the BVA stimulator capsule are illustrated in Figure 1. (a) and laser welding in (b).

Finding a sealant material for diamond is challenging principally because of the inertness that makes it so attractive as a biomaterial. [2, 9] Whilst growing a diamond film over the joint

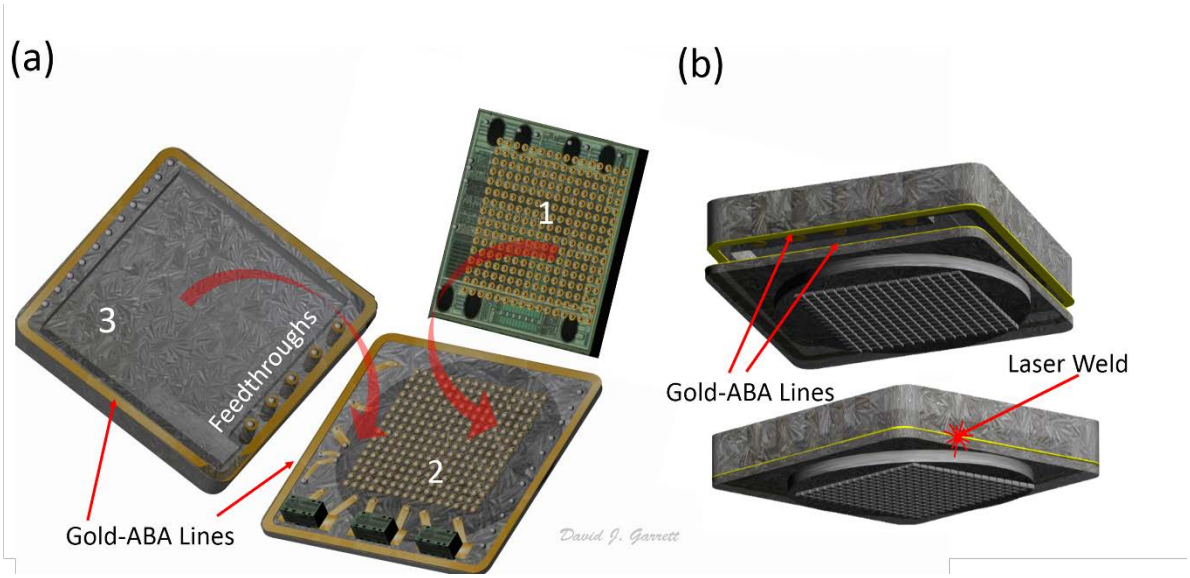

Fig. 1. (a) Components of the BVA diamond/gold encapsulation with high-density diamond electrode array (2) flip-chip bonded to a bespoke 256 channel stimulator application specific integrated circuit (ASIC) (1) and a diamond box with integrated feedthroughs for power and data transfer (3). The two diamond components are sealed by welding around the outer edges of the braze seam (b).

between capsule and electrode array would form a robust hermetic seal, the growth temperatures inside a CVD reactor are too high (400°C - 1000°C) and would destroy modern CMOS electronics. [21, 22] The abrasives industry makes use of active brazing to join synthetic diamond pads to metallic tool surfaces. Active brazes differ from conventional brazes by the inclusion of a metal solute that can chemically react with and bond to the target substrate. In the case of active brazes for diamond, this is typically a metal that can form carbides such as titanium, chromium, or vanadium. The carbide layer is credited with improving bond strength by mitigating stresses developed through mismatch of coefficients of thermal expansion between the diamond (~1×10^{-6} K^{-1}) [23] and braze alloy (15-20 $\times 10^{-6}$ K^{-1}). [24] Active brazing is also used by the medical device industry to form hermetic seals between feedthrough array and capsule using conventional ceramic materials.

The diamond / gold hermetic encapsulation reported here makes use of active braze materials in two distinctly different ways.

(i) Formation of a low number of low resistance hermetic feedthroughs in the capsule for the purposes of power and data transfer to and from the encapsulated ASIC (indicated in Figure 1).

(ii) Formation of inlaid braze lines for hermetically joining two diamond components (indicated in Figure 1).

The high electrical resistivity of diamond is an advantage for low resistance feedthroughs as conducting feedthroughs can be formed directly in the diamond, without the need for an electrically insulating insert as normally required to isolate feedthroughs in metallic encapsulation materials. For hermetically joining diamond, braze rings are formed in the two surfaces to be joined. The electronics cargo is shielded from the high temperatures of brazing by introduction to the capsule cavity after the braze process is complete, and the capsule is sealed in a final step at ambient temperatures using laser microwelding of the braze layers. To the authors' knowledge, there is no literature showing that braze joints in diamond can be hermetic or biocompatible. Here we show a method to make weldable braze layers and conductive vias in diamond capsules and demonstrate their hermeticity, durability and biocompatibility.

Methods

Fabrication of Diamond Capsule, Inlaid Braze Lines, and Braze Feedthroughs

Polycrystalline diamond (PCD) plates, either 0.25 or 0.5 mm in thickness, were patterned using a 2.5 W Nd:YAG, 532nm wavelength, nanosecond pulsed laser micromachining system (Oxford Lasers). For testing of hermetic feedthroughs, 0.25 mm thick diamond plates were prepared with four identical 150 µm diameter holes positioned near the centre of the plate. For inlaid braze lines, 50 µm deep square grooves were cut into the PCD. Graphite debris, formed during laser cutting, was removed by etching in a hydrogen plasma or by boiling in a mixture of $NaNO_3/H_2SO_4$ (conc) 1 mg/mL. An adhesion layer was created by melting Silver-ABA paste (Ag 92.75%, Cu 5%, Al 1%, Ti 1.25%, Wesgo Ltd.) over the PCD surface on a resistively-heated element under vacuum of at least 10^{-5} mbar. After the braze was observed to melt and spread (approximately 950°C), the temperature was raised to ~1000°C and held to evaporate excess Silver-ABA. The evaporation rate of Silver-ABA was monitored with a quartz crystal monitor. The sample temperature was reduced slowly once

the evaporation rate dropped to near zero. The thickness of the Silver-ABA adhesion layer was measured by scanning electron microscopy (SEM, JEOL JSM 510) of a cross section of the interface between Silver-ABA and PCD. Samples for cross sectional imaging were prepared using a focused ion beam scanning electron microscope (FIBSEM, FEI XT Nova NanoLab 200) or the abovementioned laser cutter. Gold-ABA paste (Au 96.4%, Ni 3%, Ti 0.6%, Wesgo Ltd.) was brazed over the adhesion layer in a vacuum (10 minutes, 1000°C). For feedthroughs, a 120 µm diameter Pt/Ir wire (A-M Systems) was threaded through a laser-machined 150 µm diameter hole. The wire was brazed into the hole using Gold-ABA over a Silver-ABA adhesion layer as described above. Excess braze was removed by mechanical polishing to leave braze in the groove or feedthrough holes only. For the hermetic capsule, inlaid braze lines were prepared in a flat lid component and a box component. The box cavity was excavated by laser milling, and the weldable gold braze edge exposed by laser cutting through the centre of the inlaid braze line. The process of forming a laser weldable inlaid braze line and a hermetic feedthrough is depicted in Figure 2.

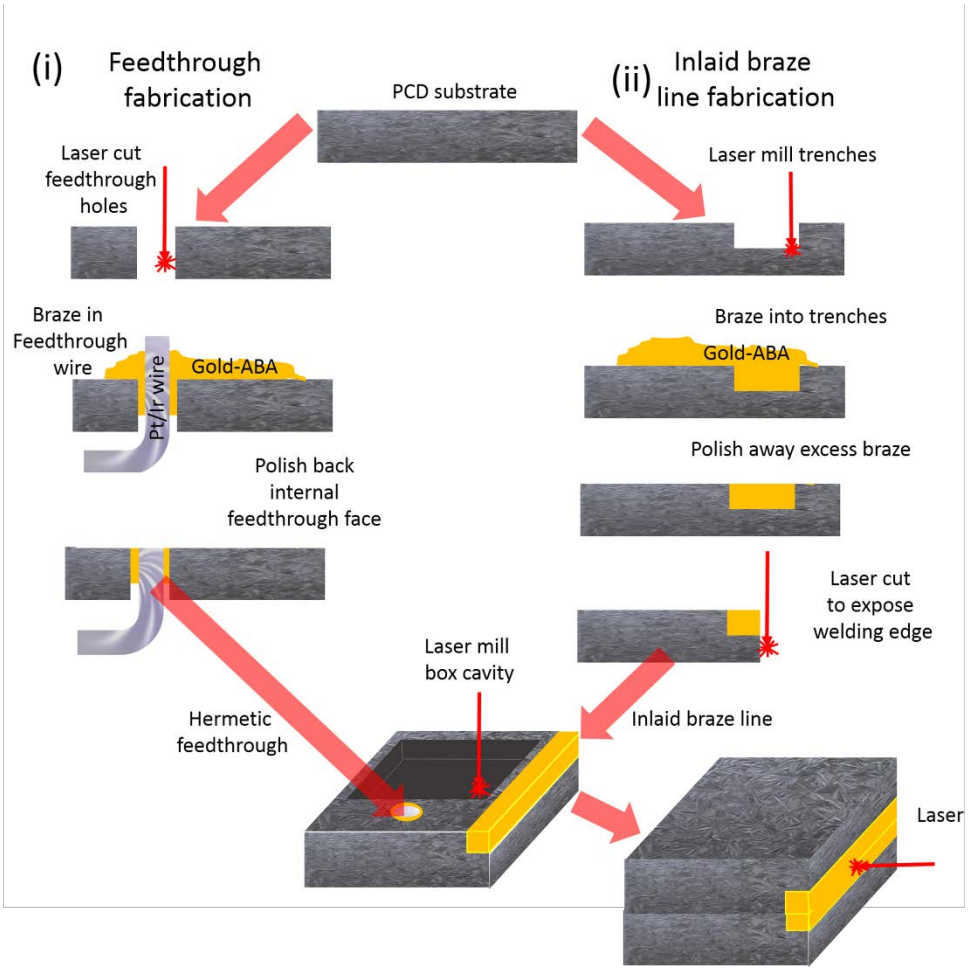

Fig. 2. Process of fabrication used for the two brazing processes, (a) hermetic feedthrough formation and (b) inlaid braze lines for hermetically joining diamond components.

Laser Welding of Inlaid Braze Lines

Inlaid gold braze lines were aligned beneath a 5 W Nd:YAG, 1064nm wavelength, microsecond pulsed laser welder with 10 µm tolerance. All laser welding was conducted through a glass window in the top of an in-house built welding chamber. The chamber was fitted with vacuum and gas inlet lines, to control the atmosphere within the chamber and with a hermetic stepper motor to rotate the sample during welding. A schematic of the chamber is included in Supplementary Figure 1.

Accelerated Ageing of Inlaid Braze

For accelerated ageing, individual samples were placed in capped sterilised glass vials containing 0.9 medical grade sterile saline (Aerowash Sterile Sodium Chloride Eyewash Solution). The vials were transferred to an environmental chamber (MicroClimate Benchtop Test Chamber Cincinnati Sub-Zero) set to 80°C for ageing. Images were recording using an

optical profiler and a SEM before and after ageing for time periods between 18 and 62 days, and compared for evidence in degradation of the braze. The hermeticity of samples containing feedthroughs was measured by the helium spray method before and after ageing.

Biocompatibility of Encapsulation Materials

Biocompatibility of silver and gold braze metals was assessed by previously established methods. For a full description and materials lists see Garrett *et al* [25] and Nayagam *et al* [26]. Briefly, 8 mm diameter diamond disks containing inlaid braze on one side were surgically inserted into the back muscle of guinea pigs for a period of 12 weeks. The diamond discs were sequestered in a silicone housing to cover the sharp edges of the diamond discs leaving only the braze-treated face exposed to the tissue. For each braze investigated, a sample was prepared where the braze covered most of the surface of the implant and a second sample type prepared where only a ring of braze 50 µm in width and 6 mm in diameter was present on the diamond surface. The second sample type was designed to better represent a welded diamond capsule which would only have a thin annulus of braze exposed. Gold-ABA samples were prepared using Silver-ABA adhesion layers. Silver-ABA rings and full sheets of a high-copper silver-based braze (Diabraze 467, Ag 68.3%, Cu 27%, Ti 4.67%) were prepared. Photographs of full Gold-ABA braze and braze ring samples are shown in Figure 3 (a) and (b) respectively. Figure 3 (c) shows the six implant locations as dashed circles, either side of a central incision through which the samples were implanted. The aim of the silicone housing was to minimise histological response arising from mechanical irritation at the edges. At the 15 week time-point the animals were euthanized and perfused. Blocks of tissue containing implants were removed and fixed. As the diamond implants are too hard to cut, the implants were removed before the tissue blocks were sectioned. The samples were stained with either Hematoxylin & Eosin (H & E) stain or Masson's Trichrome Stain in order to identify cell phonotypes present at the sample / tissue interface. Histopathological responses to the various implants were assessed by an expert pathologist under a high resolution microscope, based on the identifiable cell phenotypes.

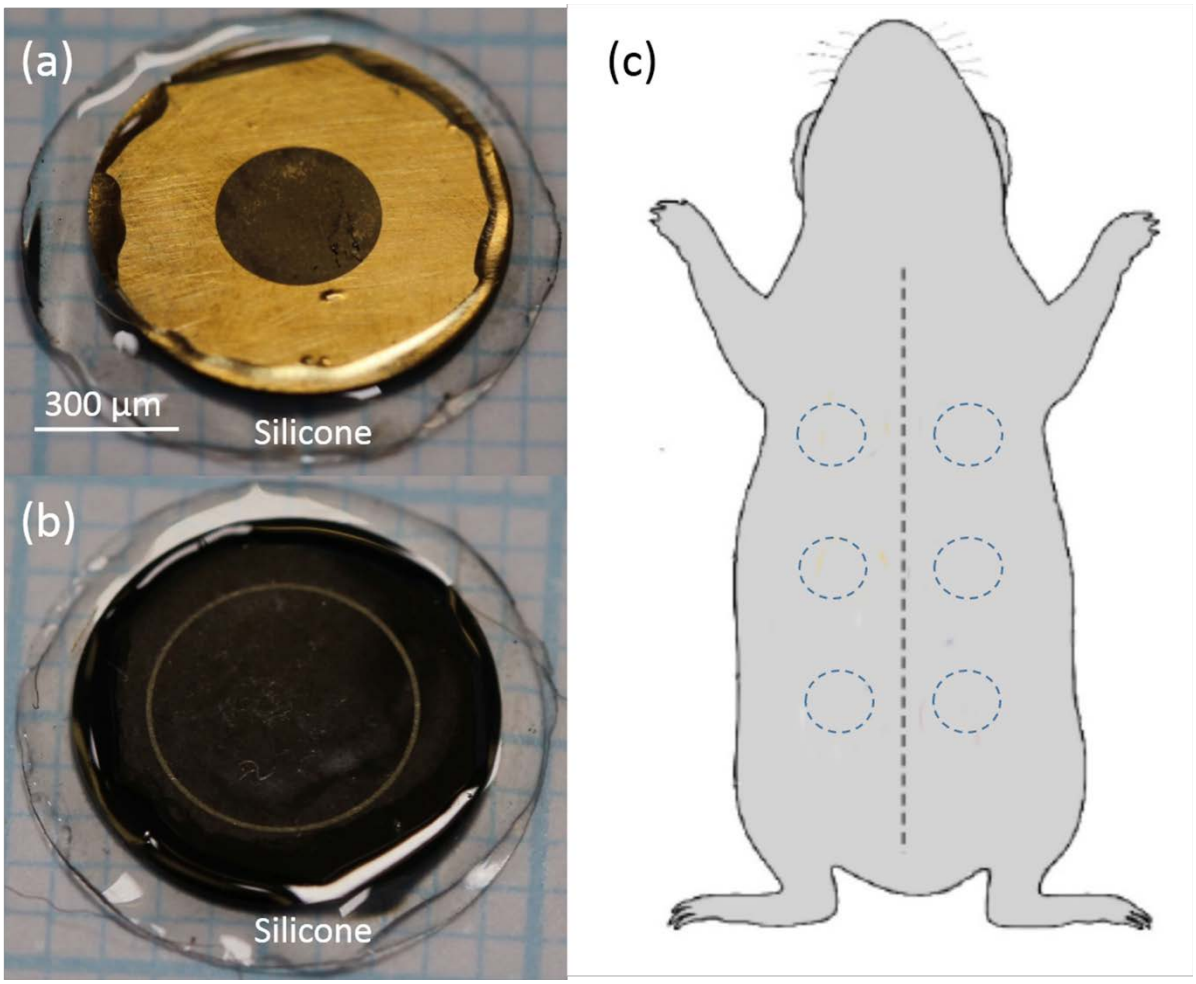

Fig. 3. (a) Full Gold-ABA braze and (b) Gold-ABA ring samples prior to surgical insertion. Braze metal is inlaid in PCD discs. Edges and reverse side are coated in medical grade silicone to avoid mechanical irritation effects. (c) The six implant locations are indicated by dashed circles. Each pair of samples were located either side of a central incision through which the samples were inserted.

Hermeticity Testing

All hermeticity tests were conducted using the spray helium leak test (MIL-STD 883J Method 1014.14 Condition A_4) and an Adixen ASM310 helium leak detector with a manufacturer-stated detection limit of 10^{-11} mbar·L/s. Hermetic vias were tested by sandwiching the sample between two O-rings, both O-rings surrounding the vias in the sample. The O-rings and sample were clamped in place such that the only potential leak path was either through the vias or through the O-rings. For welded capsules the technique required laser cutting a small hole in one wall of the capsule. The hole was sealed to the inlet of a helium leak detector using a Viton O-ring so that external helium could only potentially

leak into the detector either through the weld seam or through the O-ring. Diagrams of the apparatus used to test the two sample types is illustrated in supplementary Figure S1.

Results

Fabrication of Diamond Capsule, Inlaid Braze Lines, and Braze Feedthroughs

Trenches and holes were cut into flat PCD sheets and the trenches and holes were filled with Gold-ABA via a two-step process. Gold-ABA does not wet diamond surfaces well therefore a Silver-ABA wetting layer was applied to the PCD structures prior to Gold-ABA brazing. The majority of the Silver-ABA was evaporated away leaving a thin layer remaining. Figure 4 (a) shows a cross sectional SEM of a typical silver adhesion layer. The average thickness of the adhesion layers was 3.0 µm with a standard deviation of 0.8 µm. Figure 4 (b) is a high magnification SEM of the Silver-ABA/PCD interfaces revealing a continuous and discontinuous interface phase. The

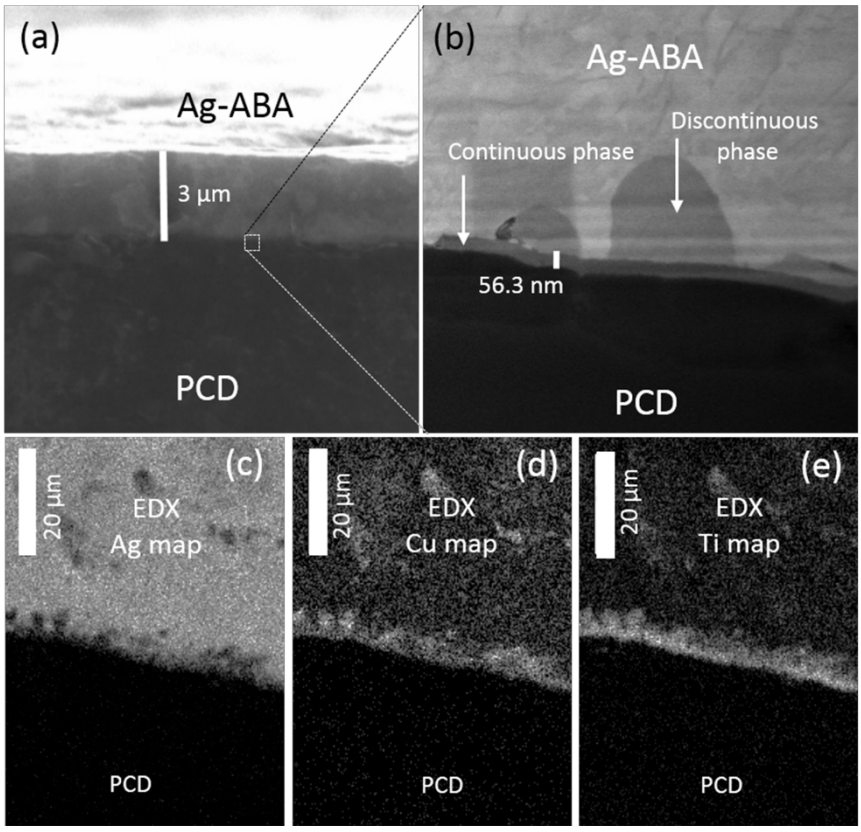

Fig. 4. Low (a) and high (b) magnification cross sectional SEM images of the interface between PCD and the Silver-ABA adhesion layer. (c), (d) and (e) are EDX maps of the distribution of Ag, Cu and Ti respectively.

continuous interface phase is thin (<100 nm) and is present across the entire interface. The discontinuous interface phase appears as discrete globules, in contact with the continuous phase. No voids were visible at the interface between the Silver-ABA and the diamond.

Figures 4 (c), (d) and (e) show the distribution of the three major components of Silver-ABA (silver, copper, titanium) established by scanning electron microscope energy dispersive X-ray spectroscopy (SEM EDX). The EDX maps indicate that silver concentration is lower at the interface and the concentrations of copper and titanium are increased at the interface.

In a separate experiment spots of Silver-ABA were melted onto a smooth PCD sample. The sample was submerged in concentrated aqua regia to dissolve away the silver. Aqua regia dissolves silver but not titanium carbide which is expected to form at the ABA/PCD interface. [27] Xray photoelectron spectroscopy (XPS) of the dissolved braze locations revealed small peaks in the C1s carbon spectra at 281.8 eV shifted 2.7 eV from the main carbon peak at 284.6 eV consistent with the Ti-C bonds. The Ti2p spectrum exhibited peaks at 455 and 460.5 eV consistent with formation of Ti-C. [28]

Gold-ABA was melted onto the Silver-ABA adhesion layers and the excess polished away leaving Gold-ABA only in the laser milled trenches or feedthrough holes in the diamond. The silver adhesion layer greatly improved the wetting of the gold-braze enabling complete filling of recesses in the PCD. Without the wetting layer we found that the molten braze tended to be ejected from the trenches in the diamond forming braze droplets on the surface of the PCD with very little remaining within the trenches. Figure 5 (a) shows an inlaid line of Gold-ABA completely filling a 60 μm deep, 300 μm wide trench cut into a 5 × 5 mm square PCD substrate. Figure 5 (b) is an SEM image depicting a cross section of the interfaces between the Gold-ABA and the PCD. The braze film conformally coats the diamond with no evidence or voids or cracks. Figure 5 (c) and (d) are SEM images of a Gold-ABA/PtIr wire feedthrough. No interface is visible between the Gold-ABA and the platinum-iridium wire, indicating excellent wetting of Pt by the braze. Development of wire connections to the external components of these feedthroughs is currently under investigation.

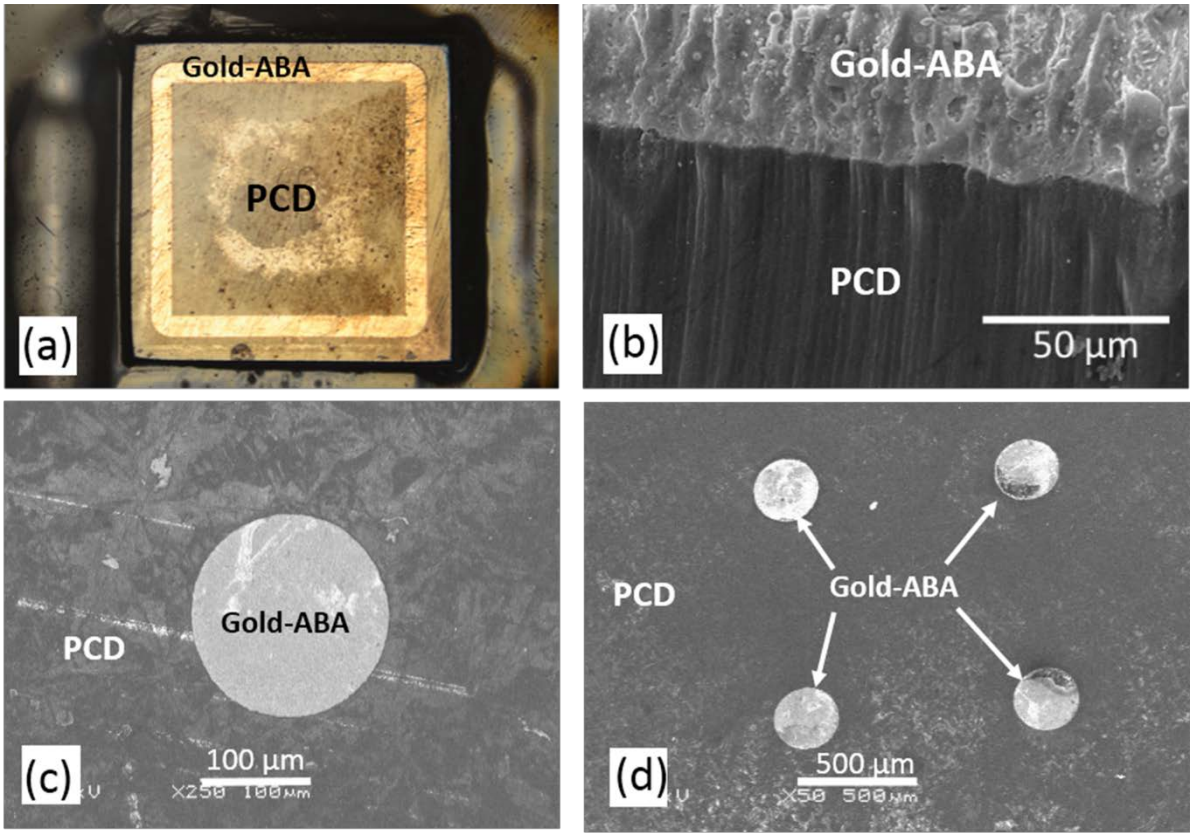

Fig. 5. (a) Optical micrograph of a polished Gold-ABA annulus formed with the aid of a Silver-ABA adhesion layer. (b) SEM image of a similar sample after laser cutting through the sample to expose a cross section of the diamond braze interface. (c) and (d) show two differing magnification top-down SEM images of 150 mm diameter Gold-ABA feedthroughs penetrating through 250 mm thick PCD sheets.

Laser Welding of Inlaid Braze Lines

Laser welding was conducted between a diamond box and lid, each featuring an inlaid braze line around the perimeter of the rim. Photographs of the box and lid are shown in Figure 6 (a) and (b). The box parts were aligned, affixed within the welding chamber and laser welded to one another forming a seal. Figure 6 (c) shows the two braze lines and diamond box parts, aligned, prior to welding. Figure 6 (d) shows a section of successfully welded Gold-ABA braze.

Following a process of optimisation, continuous welds with no visible defects could be obtained. Even with optimised parameters however a low number of defects occurred on some samples. Typically, a finished box featuring a 16 mm long perimeter weld line contained approximately 0-6 visible small defects in the weld. The most common of these

were; small round holes occurring at the centre of the weld seam (Figure 6 (e)) and/or crack formation at the Gold-ABA/PCD interface (Figure 6 (f)). For small holes a small spot weld could be used to close the hole in some cases.

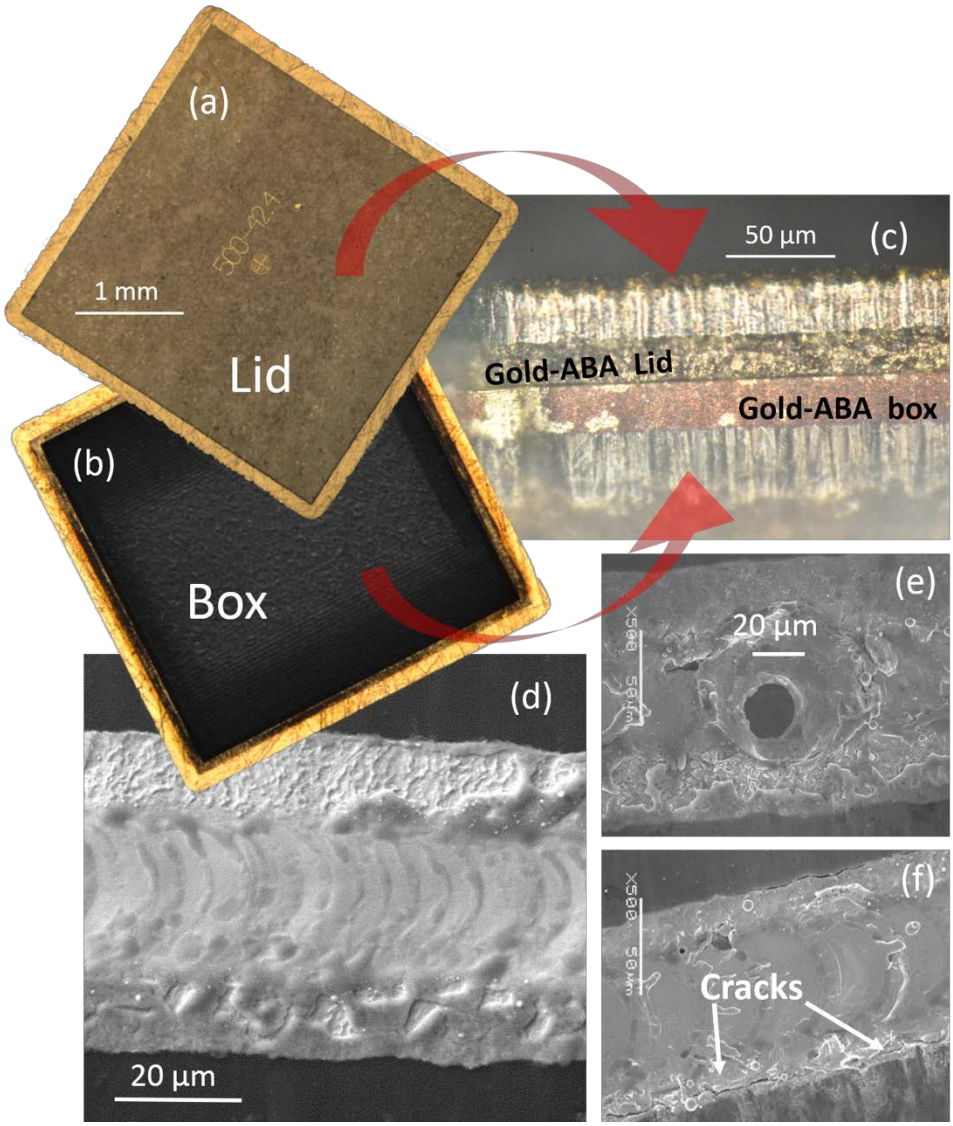

Fig. 6. Photograph of a box (b) and box lid (a) showing the inlaid braze weld line and (c) the two box parts aligned and held together, before welding. A SEM image of a successful weld seam is shown in (d) and the two most common defects, holes and cracks are shown in (e) and (f) respectively.

Accelerated Ageing and Hermeticity Testing

An inlaid ring of Gold-ABA on diamond with a 8 mm outer diameter and 1 mm inner diameter, 5 diamond/platinum wire feedthrough samples and 1 hermetic welded diamond box were aged at 80°C in 0.13 M sterile NaCl. The Gold-ABA disc was aged for 62 days and the

feedthroughs and box were aged for 24 days. The real time equivalent for 62 and 24 days is approximately 42 and 16 months respectively, calculated using the Arrhenius methods outlined in International Standard, ISO-11607 (Packaging for terminally sterilized medical devices). The calculation assumes a reaction rate factor (Q_{10}) of 2 and ambient (implanted) temperature of 37°C. Figure 7 shows microscope images (a) and (b) of the Gold-ABA sample at two magnifications depicting laser-cut reference marks in the gold braze. Figure 7 (c) shows SEM images of the laser cut line before and after ageing and Figure 7 (d) shows optical profiler images recorded before and after ageing depicting the sample topography. No differences could be discerned between the before- and after-ageing images. Small sharp edges produced during laser cutting or polishing of the braze were unaffected by the ageing process and the height difference between the diamond surface and the adjacent braze did not change. Similarly, no changes were evident in the feedthrough samples or the brazed hermetic box after ageing.

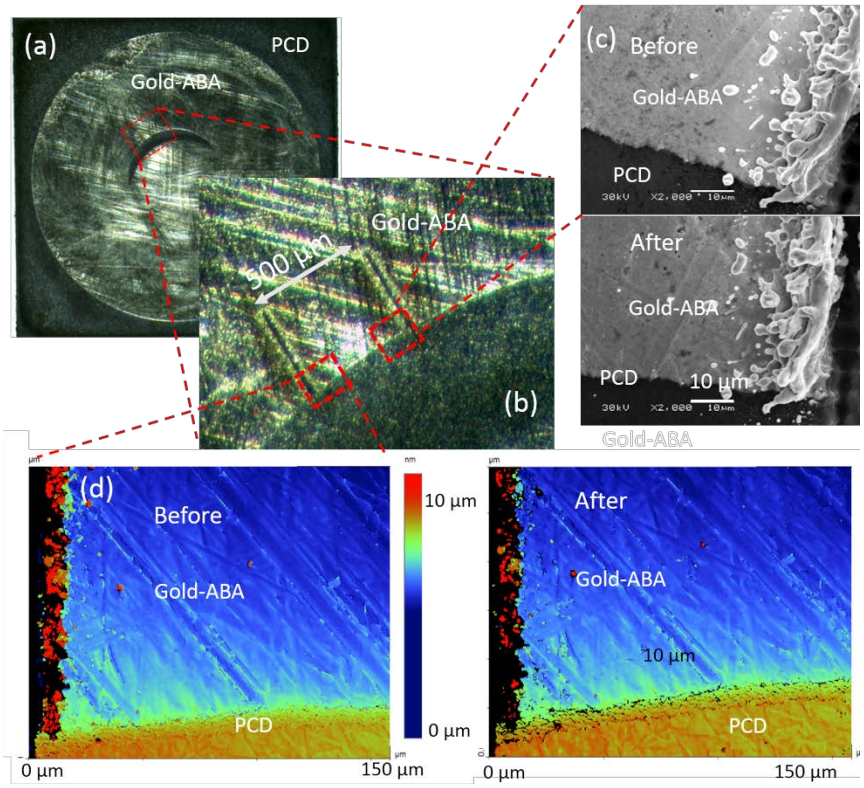

Fig. 7. (a) and (b) two magnifications of the Gold-ABA disc sample indicating laser cut reference marks. SEM images recorded before and after ageing (c), from the right hand side of the reference area. Optical profiler images (d) from the left hand side of the reference area are also shown.

Figure 8 shows a typical trace recorded from the helium leak detector during testing of a feedthrough sample. Helium is introduced over the sample at the beginning of the test window. Large leaks result in an immediate sharp spike in helium detection. Small leaks (10^{-9} – 10^{-7} mbar·L/s) result in a visible perturbation of the linear trace. An undisturbed line, such as the one depicted in Figure 8, indicates that the helium leak rate is below the detection limit of the experiment (10^{-10} mbar·L/s). After 10-20 s of helium flow over the sample, the O-ring forming the seal over the sample becomes saturated and the helium leak rate increases predictably.

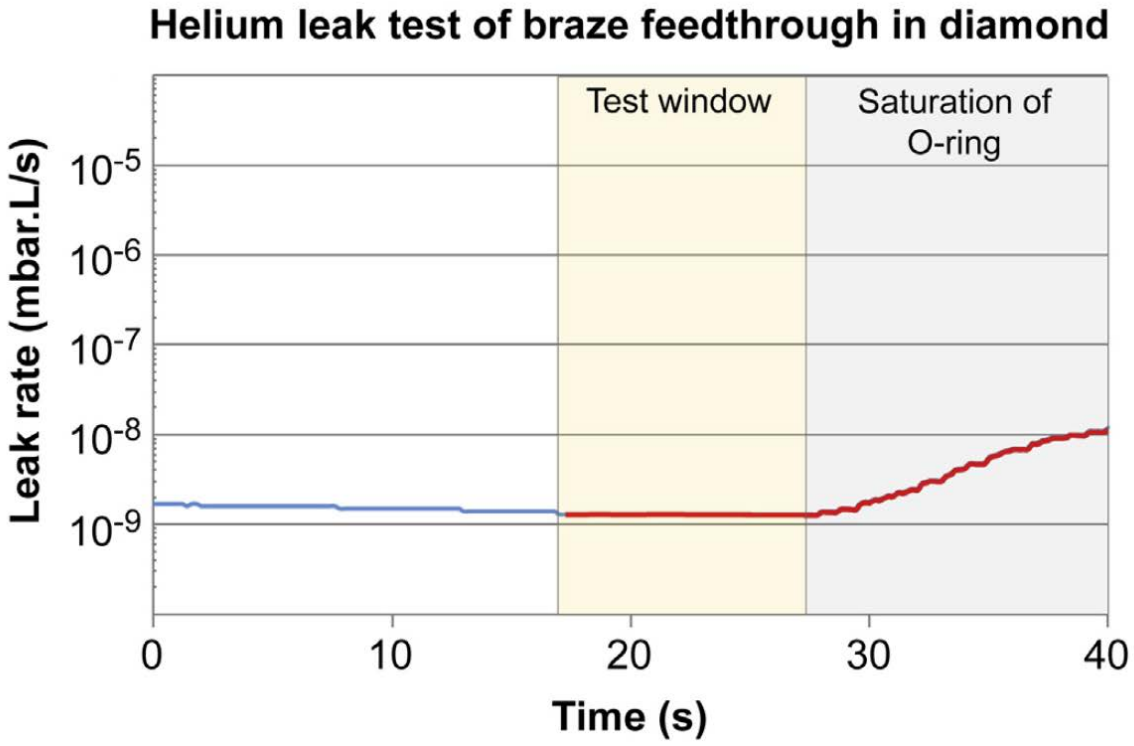

Fig. 8. Helium leak trace recording during testing of feedthrough sample indicating that the sample has no detectable leak. After several seconds of exposure to helium, the O-ring becomes saturated with helium creating a characteristic slow increase in the leak rate which is categorically different from the presentation of a test sample with a gross or fine leak.

In all cases, samples that were hermetic before ageing were hermetic after ageing. One of the five feedthrough sample exhibited a barely detectable fine leak (~ 10^{-9} mbar·L/s). The leak rate following ageing was comparable indicating that the leak path had not grown in size during the ageing process.

Histocompatibility of Encapsulation Materials

Samples of Gold-ABA, Silver-ABA and Diabraze 467 were implanted into the back muscle of Guinea pigs for a period of either 12 or 15 weeks. Following histopathological processing of the implantation sites, the histocompatibility of the brazes was assessed relative to medical grade silicone and PCD as negative controls and a piece of diamond treated with a stannous octoate solution (a metal complex known to cause a strong histopathological response) as a positive control. The relative histocompatibility was established by comparing the thickness of the gliotic capsule covering the face of the implants and by analysis of the tissue adjacent to the diamond by a specialist pathologist. The pathologist scored each section from 0 (no response) to 4 (severe response) in the three categories; acute, chronic and foreign body response based on the identifiable cell types present. Figure 9 (a) and (b) shows Trichrome-stained sections previously containing full Gold-ABA braze (a) and full silver Diabraze 467 (b) samples. The location of the samples before removal is indicated by the red dotted line in Figure 9 (a). Fibrotic encapsulation appears blue after processing and is evident on both of the samples depicted. The fibrotic encapsulation over the full Gold-ABA was thin and comparable to the control materials employed (medical grade silicone and PCD). Full silver samples

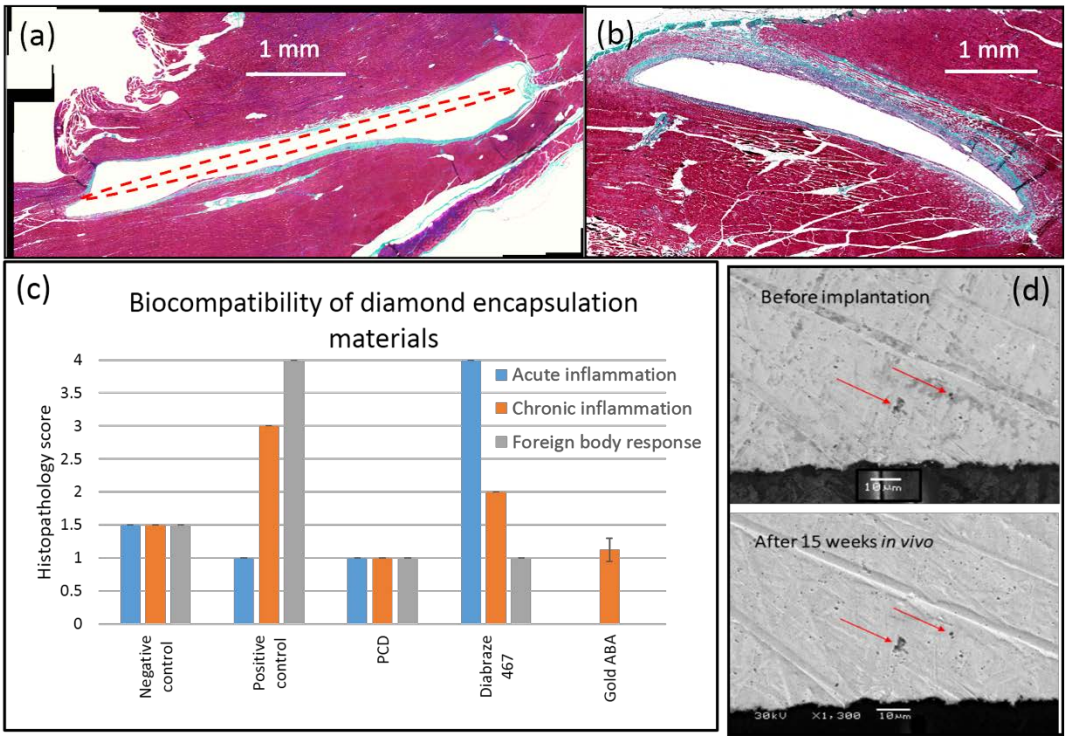

Fig. 9. (a) Histological section previously containing a full gold braze sample. (b) A histological section previously containing a full silver braze sample. The location of the

sample prior to being removed is indicated by an asterisk in both (a) and (b). (c) Pathologist scores for implanted materials: silicone (negative control), stannous octoate (positive control), PCD, silver braze, and gold braze. (d) SEM images of Gold-ABA braze before and after implantation for 15 weeks. The red arrows indicate small defects in the braze that did not
change in size or shape during the implantation period. (For interpretation of the references to colour in this figure legend, the reader is referred to the web version of this article.)

however clearly caused an increase in fibrotic encapsulation. The collated pathologist scores for the full silver Diabraze 467 samples was 4 (acute), 2 (chronic), and 1 (foreign body response) indicating a severe histopathological reaction. The pathologist scores for the collated Gold-ABA samples are tabulated in Figure 9 (c) indicating no evidence of acute response, low (1.2 ± 0.2) chronic response and no foreign body response. Both gold and silver braze ring samples produced minimal histopathology, presumably due to only having a limited amount of braze material on the samples. Therefore analysis focused on the full braze samples.

The implanted braze samples were closely examined before and after implantation. Minute topographical features in the Gold-ABA samples formed during the polishing process were unchanged over the 15 weeks, as shown in Figure 9 (d). For example, two small voids in the braze, indicated by red arrows, are clearly visible before and after implantation. The size shape and sharpness of these small features did not change during the 15 week period indicating excellent biostability of the Gold-ABA braze. In contrast, Diabraze 467 samples were visibly corroded following the implantation period.

Discussion

Silver-ABA was chosen as an interface layer to bond to diamond because of its success in the tooling industry binding diamond to metal surfaces. [29, 30] A key study comparing braze metals in joints between single crystal diamond blocks showed that Silver-ABA had highest bond strength out of a range of silver-based, copper-based and nickel-based braze alloys. [29] Silver-ABA spreads on and adheres exceedingly well to PCD but the histocompatibility results and evidence of corrosion presented here clearly render silver based brazes unsuitable

as an exposed material in a biomedical implant. When used as a wetting layer for gold based brazes however the quantities of silver employed were very low and the silver is encapsulated beneath the gold and therefore not exposed to tissue. Without Silver-ABA wetting layers, Gold-ABA tended to be ejected from laser cut features in the diamond, beading into droplets that adhered strongly to the PCD surface. The cross-section of the interface between a thick Silver-ABA layer and PCD show that the Silver-ABA formed a continuous reaction layer of several tens of nanometres' thickness, which is consistent with the titanium carbide layers observed by others in the literature. [27, 31, 32] Secondary phases formed near the interface in the Silver-ABA may be a metallic phase rich in titanium and copper. It has been shown in the literature that the titanium and copper migrate toward the reaction interface, [33] increasing concentration and thus the likelihood that precipitates will form. Forming a thin Silver-ABA layer was important as thick layers exerted strong forces upon cooling causing the diamond to bow, or crack. Thin Silver-ABA layers were achieved by evaporating excess metal during the brazing step. It is suspected that this also resulted in a change in chemical composition, with silver evaporating faster leading to a concentrated, layer of titanium-copper alloy on the diamond surface. The Gold-ABA spread well on this interlayer and exhibited greatly improved filling of laser milled features in the diamond.

Laser milling of grooves in diamond, back filling with braze and polishing proved an effective method for generating surfaces suitable for laser welding. An important design feature for laser weldable joints is that the surfaces to be welded are smooth, flat, and close together with a maximum air gap between them less than 20% of the laser beam diameter. In this case, the seams were welded with a laser beam of 50 μm diameter, so the air gap tolerance was ~10 μm. By embedding gold braze into the flat diamond surface, the metal could be ground back and polished to a roughness of <1 μm whilst staying parallel to the plane of the device. The polishing also removed braze from other areas on the diamond electrode array and capsule lid with braze feedthroughs, preventing short circuits between conducting elements. The extreme hardness of diamond is advantageous in this application because the polishing stops at the diamond surface meaning the component thickness tolerances are dictated by the thickness of the diamond. Though occurring infrequently relative to the length of the weld seam, the low number of hole and crack defects that occurred still present a significant problem. Even a single 20 um hole in the weld seam is sufficient to create a gross leak. Furthermore some samples with no visible defects proved to exhibit fine leaks ($<10^{-7}$ mbar·L/s) upon testing. The braze feedthroughs in the capsule were

designed for transmission of data and power to the encapsulated ASIC, and as such require low resistance. Hence the all-diamond high-density N-UNCD feedthroughs used in the electrode array for tissue stimulation were not suitable, however on the capsule component there is no such density limitation. Thus the feedthroughs were able to incorporate a 120 μm diameter Pt/Ir (9:1) wire, which at a length of 0.5 mm would result in a low maximum feedthrough resistance of 0.01Ω, suitable for delivering power to a stimulator circuit. The work described in this article demonstrates that fabrication of hermetic, laser welded Gold-ABA/diamond capsules is possible, though some further optimisation will be needed before the process is industry-ready.

Feedthroughs and capsules that were shown to be hermetic were aged in an environmental chamber and retested with the spray helium leak test. After 24 days at 80°C, the test samples were still hermetic. Accelerated ageing at this rate correlates to a lifetime of 16 months at 37°C using a Q_{10} factor of 2. Under this assumption, the braze joints would retain their hermeticity for over a year at physiological temperatures. Durability of the materials was also probed in the *in vivo* study. After an implantation time of 15 weeks the Gold-ABA surface showed no changes in morphology. Scratch marks and sharp ridges, which would be first to erode due to increased surface area and are highlighted in figure by red arrows, are unaffected by any acute or chronic immune response. This is consistent with gold's high inertness. Gold-ABA is almost pure gold, with alloying elements making up less than 4% of the chemical composition. Gold-ABA is also known to be resistant to harsh chemical conditions, such as in solid oxide fuel cells. [34] The complete lack of corrosion demonstrated by Gold-ABA aged for 62 days at 80°C (real time equivalent 42 months) indicates that Gold-ABA hermetic seals are very likely to be long lasting. Extended high temperature ageing studies will be required however to establish the long term (10-50 y) performance of the materials.

Biocompatibility is a loosely-defined property of materials destined for contact with living tissue. It can cover a range of effects that a material can have on the body, from clotting to toxicity to carcinogenicity. The recommended test battery of tests to gain approval for a new material to be included in Class III medical devices is lengthy and expensive, but worthwhile when a particular materials paradigm is falling short of an important future need. The study performed here testing the immune response in the dorsal muscle of a guinea pig is an important pilot test of histocompatibility, showing that these materials are worthy of further investigation. Histology results from the implant sites of PCD coated with Gold-ABA on a Silver-ABA adhesion layer showed that the Gold-ABA braze metal is comparable to medical

grade silicone in terms of degree of fibrotic encapsulation and acute, chronic and foreign body response. The experiment was performed as a continuation of an earlier study by the same team investigating the histocompatibility of PCD, N-UNCD and boron-doped PCD, and can be directly compared to the positive control using stannous octoate. This material causes a severe inflammatory response and due to ethical concerns it was deemed unnecessary to repeat it in the current study. The thickness of the fibrous encapsulation surrounding the braze-coated implant was low compared to the silicone-coated control. It was noted however that there was some unexplained foreign body response on the silicone-coated side of the Gold-ABA implants (not the gold-coated side). The Gold-ABA surface area exposed to the tissue in full braze samples was much greater than what would be exposed in a device, since the weld seams are narrow, the feedthroughs are small, and the device would be encapsulated in medical grade silicone. Therefore this very much a worst case scenario concerning the biocompatibility the diamond/gold braze encapsulation design. The histocompatibility results and accelerated ageing indicate that the inclusion of the Silver-ABA adhesion layer and Gold-ABA alloying elements do not change behaviour significantly from that of pure gold. Either the Silver-ABA did not mix with the Gold-ABA, or the concentrations of the non-gold solutes were low enough to be inconsequential, with the gold alloy retaining its chemical inertness.

Conclusions

A new hermetic encapsulation paradigm for a high resolution bionic eye, using polycrystalline diamond, was presented. The new packaging technology uses high-conductivity gold braze feedthroughs for power and data input and a laser welded seam of Gold-ABA braze joining the diamond shell components.

Braze features were added to the PCD capsule components by laser cutting grooves, melting braze into them and polishing away excess braze. A thin adhesion layer of Silver-ABA was used to improve the wetting of Gold-ABA on diamond permitting complete filling of laser milled features in the diamond. Mechanical polishing created ideal surfaces for welding and electrically isolated braze feedthroughs.

Spray helium leak tests showed that successfully welded components had no detectible helium leak rate. Accelerated ageing in an environmental chamber demonstrated that Gold-ABA did not corrode over a real time equivalent period of 42 months nor was there any

evidence of corrosion during 15 weeks of implantation in a guinea pig. Welded boxes and feedthroughs remained hermetic after a real time equivalent of 16 months of ageing. Implanting Gold-ABA coated PCD discs in the dorsal muscle of guinea pigs for 15 weeks caused minimal immune response within the adjacent tissue, suggesting that the material is both biostable and histocompatible. Conversely silver-based braze caused a severe tissue reaction and visibly corroded during implantation and accelerated ageing experiments. We conclude that silver based brazes are not suitable as exposed materials in biomedical implants both in terms of biocompatibility and longevity. Silver-ABA however when used as an adhesion layer for Gold-ABA did not appear to negatively impact on the histocompatibility or longevity of that material.

Freestanding diamond hermetic encapsulations have the potential to open up possibilities for range of new-generation bionic devices that interact with the body in complex ways. As understanding of retinal, cortical and other systems increases, such technologies could be leveraged for precise stimulation and recording of large numbers of neurons with devices that will last for the lifetime of the user. In the near term, the diamond encapsulation provides a solution to the challenge of a high density retinal prosthesis, with the aim of restoring high resolution vision to the blind.

Acknowledgements

This research was supported by the Australian Research Council through its Special Research Initiative (SRI) in Bionic Vision Science and Technology grant to Bionic Vision Australia (BVA). The authors wish to acknowledge the facilities and the scientific assistance of the Australian Microscopy & Microanalysis Research Facility at the RMIT. DJG is supported by an Australian Research Council (ARC) DECRA grant DE130100922. The Bionics Institute acknowledges the support received from the Victorian Government through its Operational Infrastructure Program.

References

[1] Menzel-Severing J, Laube T, Brockmann C, Bornfeld N, Mokwa W, Mazinani B, et al. Implantation and explantation of an active epiretinal visual prosthesis: 2-year follow-up data from the EPIRET3 prospective clinical trial. Eye. 2012;26:501-9.

[2] Wise K, Anderson D, Hetke J, Kipke D, Najafi K. Wireless implantable microsystems: high-density electronic interfaces to the nervous system. Proceedings of the IEEE. 2004;92:76-97.

[3] Rodger DC, Fong AJ, Li W, Ameri H, Ahuja AK, Gutierrez C, et al. Flexible parylene-based multielectrode array technology for high-density neural stimulation and recording. Sensors and Actuators B. 2008;132:449-60.
[4] Margalit E, Maia M, Weiland JD, Greenberg RJ, Fujii GY, Torres G, et al. Retinal Prosthesis for the Blind. Survey of Ophthalmology. 2002;47:335-56.
[5] Weiland JD, Humayun MS. Visual Prosthesis. Proceedings of the IEEE. 2008;96:1076-84.
[6] Rizzo JF, III. Update on Retinal Prosthetic Research: The Boston Retinal Implant Project. Journal of Neuro-Ophthalmology. 2011;31:160-8.
[7] Guenther T, Lovell NH, Suaning GJ. Bionic vision: system architectures -a review. Expert Review of Medical Devices. 2012;9:33-48.
[8] Kelly SK, Shire DB, Chen J, Doyle P, Gingerich MD, Cogan SF, et al. A Hermetic Wireless Subretinal Neurostimulator for Vision Prostheses. IEEE Transactions on Biomedical Engineering. 2011;58:3197-205.
[9] Gill EC, Antalek J, Kimock FM, Nasiatka PJ, McIntosh BP, Tanguay ARJ, et al. High-density feedthrough technology for hermetic biomedical packaging. MRS Proceedings. 2013;1572.
[10] Guenther T, Kong C, Lu H, Svehla MJ, Lovell NH, Ruys A, et al. Pt-Al2O3 interfaces in cofired ceramics for use in miniaturized neuroprosthetic implants. Journal of Biomedical Materials Research Part B: Applied Biomaterials. 2014;102:500-7.
[11] Ordonez JS, Schuettler M, Ortmanns M, Stieglitz T. A 232-channel retinal vision prosthesis with a miniaturized hermetic package. Engineering in Medicine and Biology Society (EMBC), 2012 Annual International Conference of the IEEE2012. p. 2796-9.
[12] Dion I, Baquey C, Monties JR. Diamond - The Biomaterial of the 21st Century? International Journal of Artificial Organs. 1993;16:623-7.
[13] Tang L, Tsai C, Gerberich WW, Kruckeberg L, Kania DR. Biocompatibility of chemical-vapour-deposited diamond. Biomaterials. 1995;16:483-8.
[14] Bajaj P, Akin D, Gupta A, Sherman D, Shi B, Auciello O, et al. Ultrananocrystalline diamond film as an optimal cell interface for biomedical applications. Biomedical Microdevices. 2007;9:787-94.
[15] Shi B, Jin Q, Chen L, Auciello O. Fundamentals of ultrananocrystalline diamond (UNCD) thin films as biomaterials for developmental biology: Embryonic fibroblasts growth on the surface of (UNCD) films. Diamond and Related Materials. 2009;18:596-600.
[16] Smisdom N, Smets I, Williams OA, Daenen M, Wenmackers S, Haenen K, et al. Chinese hamster ovary cell viability on hydrogen and oxygen terminated nano- and microcrystalline diamond surfaces. Physica Status Solidi A - Applications and Materials Science. 2009;206:2042-7.
[17] Xiao X, Wang J, Liu C, Carlisle JA, Mech B, Greenberg R, et al. In Vitro and In Vivo Evaluation of Ultrananocrystalline Diamond for Coating of Implantable Retinal Microchips. Journal of Biomedical Materials Research Part B: Applied Biomaterials. 2006;77B:273-81.
[18] Garrett DJ, Ganesan K, Stacey A, Fox K, Meffin H, Prawer S. Ultra-nanocrystalline diamond electrodes: optimization towards neural stimulation applications. Journal of Neural Engineering. 2012;9.
[19] Hadjinicolaou AE, Leung RT, Garrett DJ, Ganesan K, Fox K, Nayagam DAX, et al. Electrical stimulation of retinal ganglion cells with diamond and the development of an all diamond retinal prosthesis. Biomaterials. 2012;33:5812-20.
[20] Ganesan K, Garrett DJ, Ahnood A, Shivdasani MN, Tong W, Turnley AM, et al. An all-diamond, hermetic electrical feedthrough array for a retinal prosthesis. Biomaterials. 2014;35:908-15.
[21] Sedky S, Witvrouw A, Bender H, Baert K. Experimental determination of the maximum post-process annealing temperature for standard CMOS wafers. Electron Devices, IEEE Transactions on. 2001;48:377-85.
[22] Takeuchi H, Wung A, Sun X, Howe RT, King T-J. Thermal Budget Limits of Quarter-Micrometer Foundry CMOS for Post-Processing MEMS Devices. IEEE Transactions on Electron Devices. 2005;52:2081-6.
[23] Element-Six. Diafilm TM Product Sheet. In: e6, editor.2013.

[24] MTC-Wesgo-Metals. Active Brazing Services & Solutions. Morgan Advanced Materials; 2009.
[25] Garrett DJ, Saunders AL, McGowan C, Specks J, Ganesan K, Meffin H, et al. In vivo biocompatibility of boron doped and nitrogen included conductive-diamond for use in medical implants. Journal of Biomedical Materials Research Part B: Applied Biomaterials. 2015:n/a-n/a.
[26] Nayagam DAX, Williams RA, Chen J, Magee KA, Irwin J, Tan J, et al. Biocompatibility of Immobilized Aligned Carbon Nanotubes. Small. 2011;7:1035-42.
[27] Huang S-F, Tsai H-L, Lin S-T. Effects of brazing route and brazing alloy on the interfacial structure between diamond and bonding matrix. Materials Chemistry and Physics. 2004;84:251-8.
[28] Tachibana T, Williams BE, Glass JT. Correlation of the electrical properties of metal contacts on diamond films with the chemical nature of the metal-diamond interface. II. Titanium contacts: A carbide-forming metal. Physical Review B. 1992;45:11975.
[29] Hsieh Y-C, Lin S-T. Interfacial Bonding Strength Between Brazing Alloys and CVD Diamond. Journal of Materials Engineering and Performance. 2009;18:312-8.
[30] Artini C, Muolo M, Passerone A. Diamond–metal interfaces in cutting tools: a review. Journal of Materials Science. 2012;47:3252-64.
[31] Klotz UE, Khalid FA, Elsener HR. Nanocrystalline phases and epitaxial interface reactions during brazing of diamond grits with silver based Incusil-ABA alloy. Diamond and Related Materials. 2006;15:1520-4.
[32] Khalid FA, Klotz UE, Elsener HR, Zigerlig B, Gasser P. On the interfacial nanostructure of brazed diamond grits. Scripta Materialia. 2004;50:1139-43.
[33] Singh M, Shpargel TP, Morscher GN, Asthana R. Active metal brazing and characterization of brazed joints in titanium to carbon-carbon composites. Materials Science and Engineering A. 2005;412:123-8.
[34] Singh M, Shpargel TP, Asthana R. Brazing of Stainless Steel to Yttria-Stabilized Zirconia Using Gold-Based Brazes for Solid Oxide Fuel Cell Applications. International Journal of Applied Ceramic Technology. 2007;4:119-33.

Supplementary Data

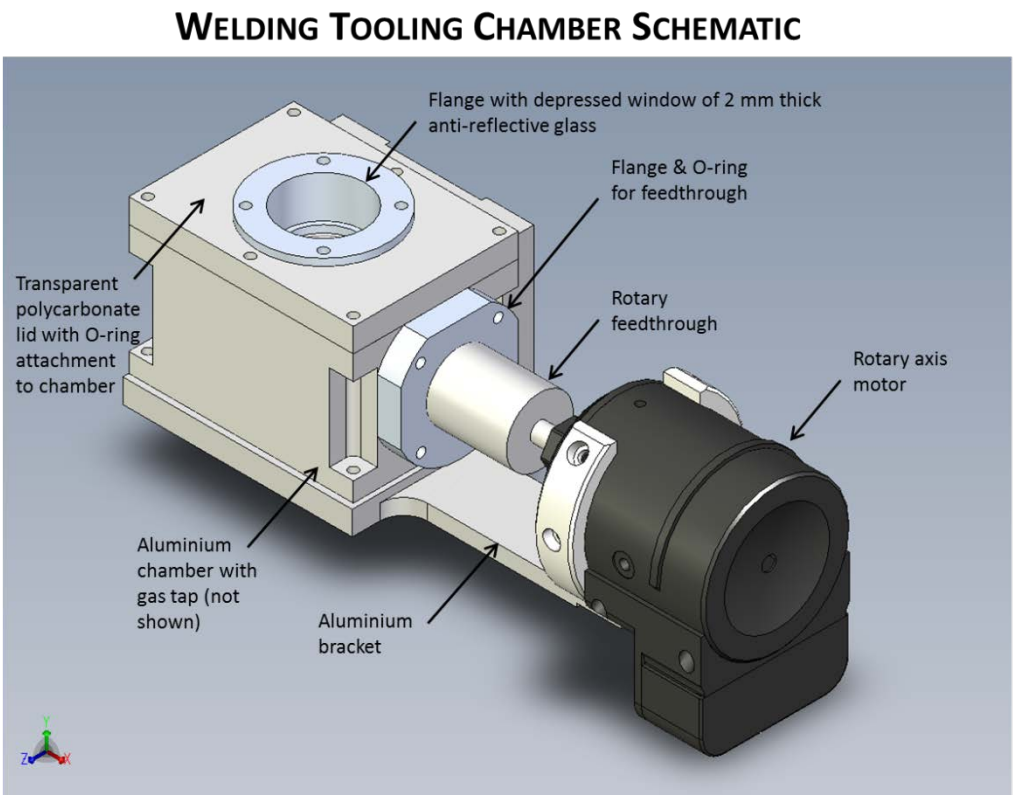

Supplementary Figure 1

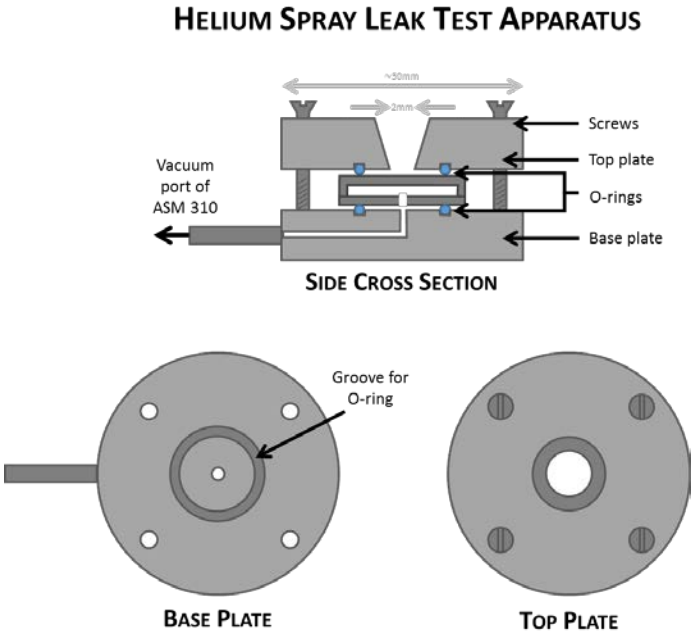

Supplementary Figure 2